Two dimensional Cu based Nanocomposite materials for Direct Urea Fuel Cell

Najrul Hussain [a], Mohammad Ali Abdelkareem [a,b, c], Hussain Alawadhi [a,d], Abed Alaswad [e]*
Enas Taha Sayed[a,c]

[a]*Center for Advanced Materials Research, Research Institute Of Sciences and Engineering, University of Sharjah, PO Box 27272, Sharjah, United Arab Emirates*
[b]*Dept. of Sustainable and Renewable Energy Engineering, University of Sharjah, PO Box 27272, Sharjah, United Arab Emirates*
[c]*Chemical Engineering Department, Minia University, Elminia, Egypt*
[d]*Dept. of Applied Physics, University of Sharjah, PO Box 27272, Sharjah, United Arab Emirates, United Arab Emirates*
[e]*School of Engineering and Applied Science, Aston University*

∗ Corresponding author at: Mohammad Ali Abdelkareem; E-mail address: (mabdulkareem@sharjah.ac.ae)

Abstract:

In this work, Cu_2O nanoparticles were successfully prepared onto the surface of two-dimensional graphitic carbon nitride ($g-C_3N_{4)}$ by using a simple solution chemistry approach. An environment-friendly reducing agent, glucose, was used for the synthesis of Cu_2O NPs onto the surface of $g-C_3N_4$ without using any surfactant or additives. The surface composition, crystalline structure, morphology, as well as other properties have been investigated using XPS, XRD, SEM, FTIR, FESEM, EDS, etc. The electrochemical measurements of the prepared materials demonstrated that Cu_2O exhibited a weak oxidation activity towards urea, while $g-C_3N_4$ has no activity towards urea oxidation. The Cu_2O supported on the surface of $g-C_3N_4$ ($Cu_2O-g-C_3N_4$) demonstrated a significant activity towards urea oxidation that reached two times that of the unsupported one. The significant increase in the performance was related to the synergetic effect between the Cu_2O and $g-C_3N_4$ support. The prepared composite materials demonstrated high stability towards urea oxidation as confirmed from the stable current discharge for around three hours without any noticeable degradation performance.

Keywords: Two dimensional (2D); Graphitic carbon nitride ($g-C_3N_4$); Cu_2O Nanoparticles (NPs); Cyclic Voltametry (CV); Electrochemical impedance Spectroscopy (EIS); Direct urea fuel cell.

1. Introduction:

Fossil fuel cannot be considered as the conventional energy source in the near future by considering the fact of availability of resources, environmental issues, and also variations in their price. In that case, renewable energy sources such as biomass energy [1], solar energy [2], ocean energy [3], wind energy [4], etc. meet the real demand for energy sources in the present scenario. Among them, biomass energy has attracted particular attention to researchers all over the world because of not only as a sustainable energy source but also as a major role in waste management [5] [6] [7] . Among different types of organic materials, which are usually biomass energy resources present in wastewater, urea is one of the major biomass energy resources because of its high energy content [10] [11] [12]. On the other hand, the development of highly effective strategies for converting biomass-derived fuel into energy is an important issue. In that case, Fuel cells are considered as proficient electrochemical technology that can directly convert chemical energy stored in different fuels into electricity [13] [14] [15]. Moreover, Fuel cells fulfill all the criteria of sustainable energy since fuel cells are very small in size, environment-friendly, and avoid unwanted sounds as compared to other devices [16] [17]. The efficiency of urea fuel cell mainly depends upon the activity of anode catalyst for the oxidation of urea. Many catalysts are developed by researchers all over the world to date for the oxidation of urea. Different types of Pt catalysts such Pt/C, Pt/rGO, Pt nanoflowers, AuPt/c, Pt/HGN are mainly found to be efficient in the oxidation of urea [18] [19]. But, Pt is not only expensive but also limited in resources. As a replacement of Pt, a large number of Ni-based catalysts such as metallic Ni, composite of Ni, and Ni alloys with different morphologies are investigated [20, 21]. For example, $Ni(OH)_2$ nanoribbons, $Ni(OH)_2$/Vulcan carbon [22], NiO/Gr [23], Ni/C [24], Ni nanotube [25], Ni nanowires [26], Ni/MWCN [27], Ni/GO [28], Ni-graphene [29], Ni-Zn [30], Ni-Co [31], Ni-Cd [32], Ni-Mn [33], Ni-Fe double hydroxide [34], $Ni/C-PbO_2$ [35], Ni-MOF [36], Ni/Co hydroxide particles [37], NiFe-LDH/MWCNTs/NF [38]

La$_2$NiO$_4$/CNTs/PANI [39], Rh-NCs/NiO nanosheet [40] etc., are used as anode electrocatalyst due to their high activity in the oxidation of urea. Although several metals such as Co, Mn, Sn are alloyed with Ni to obtain significant improvement of the catalytic activity of Ni, few active Ni free non-precious catalyst are reported. Therefore, searching a Ni-free nonprecious catalyst for urea oxidation is of great importance. In that case, a very few Cu based catalyst are reported for electrooxidation of urea as a replacement of Ni-based catalysts. Shi et al. synthesized Cu(OH)$_2$ nanowire on copper foam for their application towards oxidation of urea. The synthesized Cu(OH)$_2$ catalyst is found to have excellent electrocatalytic activity along with high stability [41]. Another work reported by Yang et al. demonstrated that Cu/Cu$_2$O catalyst exhibited high catalytic activity in the electrolysis of urea [42]. In this study, Cu$_2$O nanoparticles are synthesized adopting simple solution chemistry approach using environment friendly reducing agent as a replacement of commonly used Ni based catalyst for their application in the oxidation of urea.

Further, the immobilization or deposition of nanoparticles on proper support can enhance their electrocatalytic activity since it can affect the shape, size, as well as distribution of the nanoparticles which in turn results in high surface to volume ratio, enhanced electronic as well as chemical properties. Although various support materials such as mesoporous silica [43], TiO$_2$ nanotubes [44] are used, two dimensional (2D) materials become particularly significant for the researchers due to their unique properties. The distinctive electronic properties and a great variety of 2D materials make them highly promising for various technological applications such as energy storage, energy conversion, electronics, transistors, optical devices, etc. [45] [46]. Typically, the research on 2D materials started in 2004 after the discovery of graphene by Novoselov and Geim [47]. The discovery of graphene with extraordinary properties invigorated research on other 2D materials beyond graphene such as transition metal chalcogenides (TMC), transition metal carbides, graphitic carbon nitride (g-C$_3$N$_4$), *h*-boron

carbon nitride (*h*-BCN) and hexagonal boron nitrides(h-BN)due to their high thermal conductivity, electrical conductivity, high mechanical strength, low toxicity, chemical inertness etc., [48] [49]. Recently, g-C_3N_4, which is the most stable allotrope and a novel metal-free polymeric semiconductor material, has engrossed extensive attention due to their layered structure, high nitrogen content, good stability, nontoxicity and interesting electronic structural properties [50] [51, 52]. In addition to these important properties, g-C_3N_4 is generally synthesized from low-cost precursors like urea, melamine, cyanamide, etc. and therefore, which make it highly valued for enormous applications like photodegradation, photocatalysis, CO_2 reduction and electrocatalysis. [53] [54] [55]. However, the semiconductor-based material like g-C_3N_4 has poor electron mobility and, as a result of which limits their electrochemical applications. In that case, enormous efforts have been devoted by the researchers towards the conjugation or development of composite materials of g-C_3N_4 with other crystalline materials like metal or metal oxide nanoparticles to enhance their electrochemical performances.

Although graphene is frequently used as support for the synthesis of nanocatalyst in urea oxidation, there is no single report of using g-C_3N_4 as support for the synthesis of anode catalyst in this particular application. Here, for the first time, g-C_3N_4 was used as a support for Cu_2O NPs for its use as electrocatalyst in the oxidation of Urea. Here, the use of g-C_3N_4 acts as not only as support for Cu_2O NPs but also it forms a new type of composite materials i.e. Cu_2O- g-C_3N_4 composite material, which enhanced their performances in the oxidation of urea due to their synergistic effect.

2. Experimental:

2.1. Materials and Methods:

Urea (Sigma-Aldrich), $Cu(CH_3COO)_2.H_2O$ (>98%, Sigma-Aldrich) Glucose (Sigma-Aldrich), Ethanol (ACS grade, Merck), NaOH (AR, 98%, SRL), KOH (AR, 85%, SRL), Isopropanol (ACS grade, Merck), D521 Nafion dispersion.

X-ray diffraction study was done with the help of D8 Advance, Bruker, X-ray diffractometer with a Cu Kα having wavelength λ = 1.54056 Å as an X-ray source. The investigation about the functional groups in synthesized samples was done using FT/IR-6300, JASCO, in the range of 400-4000 cm^{-1}. X-ray photoelectron spectroscopy (XPS) spectra were obtained from a ESCALAB 250 (Thermofisher) electron spectrometer along with a hemispherical sector energy analyzer. Monochromatic Al Kα X-ray source was used at a source excitation energy of 15 KeV and an emission current of 6 mA. The surface morphology, as well as the elemental composition of the synthesized samples, were examined with the help of Field Emission Scanning Electron Microscopy FESEM (Fei Apreo C, Czech Republic) and Energy Dispersive Spectroscopy (Oxford Instruments, United Kingdom), respectively.

2.2. Electrochemical measurements:

The electrochemical performances of the synthesized materials were investigated using a three-electrode cell, where Pt foil was used as a counter electrode, Ag/AgCl electrode as the reference electrode, and glassy carbon electrode as a working electrode. Catalyst ink was prepared from the dispersion of the desired amount of the synthesized catalyst in a mixture of Nafion solution and isopropanol in an ultrasound bath for a certain time. Then, different volumes of the catalyst ink on the surface of a glassy carbon electrode were used to give catalyst loading of 1.4, 2.8, 4.2, and 5.6 $mgcm^{-2}$. The working electrode was left to dry in air for 30 minutes, and then it was dried at 50 °C overnight. After that, cyclic voltammetry and chronoamperometry measurements of all the samples were done using VersaStat 4, USA potentiostat. Various concentrations like 0.1 M, 0.33 M, 0.5 M, 1 M and 2 M of urea were made in 1 M KOH for the measurement. Electrochemical impedance spectroscopy (EIS) analysis was made with the help of Biologic VSP-200 instrument by considering 100 kHz to 50 mHz as the range of the frequency.

2.3. Synthesis of the graphitic carbon nitride (g-C₃N₄):

A silica crucible containing 15 g of urea was kept in a Tubular Furnace, and the sample was heated at 550 ºC for 3 h at a ramping heat of 5 ºC. Finally, a product of $g-C_3N_4$ having yellow color is obtained.

2.4. Synthesis of Cu₂O nanoparticles:

A solution of $Cu(CH_3COO)_2$. H_2O (0.35g dissolved in 20 mL water +15 mL Ethanol) was prepared in a 100 mL round bottom flask. After that, an aqueous solution of glucose (0.8 g in 10 mL water) was added slowly, followed by the addition of NaOH (100 mg). The whole reaction mixture was heated to 70 °C for 3 h until the appearance of a solid product. The solid product was obtained by centrifugation and then washed with water as well as ethanol many times, and after that, it was dried at 60 °C.

2.5. Synthesis of Cu₂O nanoparticles onto g-C₃N₄ (Cu₂O-g-C₃N₄ composite):

A solution of $Cu(CH_3COO)_2$. H_2O (0.35g dissolved in 20 mL water +15 mL Ethanol) was prepared in a 100 mL round bottom flask. Then a 20 mL suspension of $g-C_3N_4$ (500 mg in 100 mL water) was added to the above copper solution. Then the reaction mixture was mechanically stirred for 15 min at room temperature. After that, an aqueous solution of glucose (0.8 g in 10 mL water) was added, followed by the addition of NaOH (100 mg). The whole reaction mixture was heated to 70 °C for 3 h until the appearance of the solid product. The solid product was collected by centrifugation and then washed with water as well as ethanol many times, and after that, it was dried at 60 °C.

3. Results and discussions:

3.1. Characterization of g-C₃N₄, Cu₂O and Cu₂O-g-C₃N₄ composite material

The synthesized g-C$_3$N$_4$, Cu$_2$O nanoparticles, and Cu$_2$O-g-C$_3$N$_4$ composite material were characterized by XRD, FTIR, FESEM, EDS, and XPS analysis. The XRD pattern of g- g-C$_3$N$_4$, as shown in Fig. 1(a) displayed two peaks at 12.8° and 27.3°, which corresponds to the (100) and (002) planes of g-C$_3$N$_4$ [56]. The peak observed at 12.8° is attributed to the in-plane repeated tri-s-triazine units in the structure of g-C$_3$N$_4$ with a *d*-spacing of 6.8 Å. Another peak observed at 27.3° is corresponds to the interlayer stacking (*d*= 3.24 Å) of conjugated aromatics segments. Moreover, the XRD pattern of Cu$_2$O (Fig.1(b)) shows the main peaks at 29.4°, 36.4°, 42.3°, 61.3° and 73.5° corresponding to (110), (111), (200), (220) and (311) crystallographic planes of cubic Cu$_2$O nanoparticles [57]. In the case of the Cu$_2$O-g-C$_3$N$_4$ composite material, the existence of XRD peaks for both g-C$_3$N$_4$ and Cu$_2$O confirm the synthesis of Cu$_2$O-g-C$_3$N$_4$ composite material (Fig.1(c)).
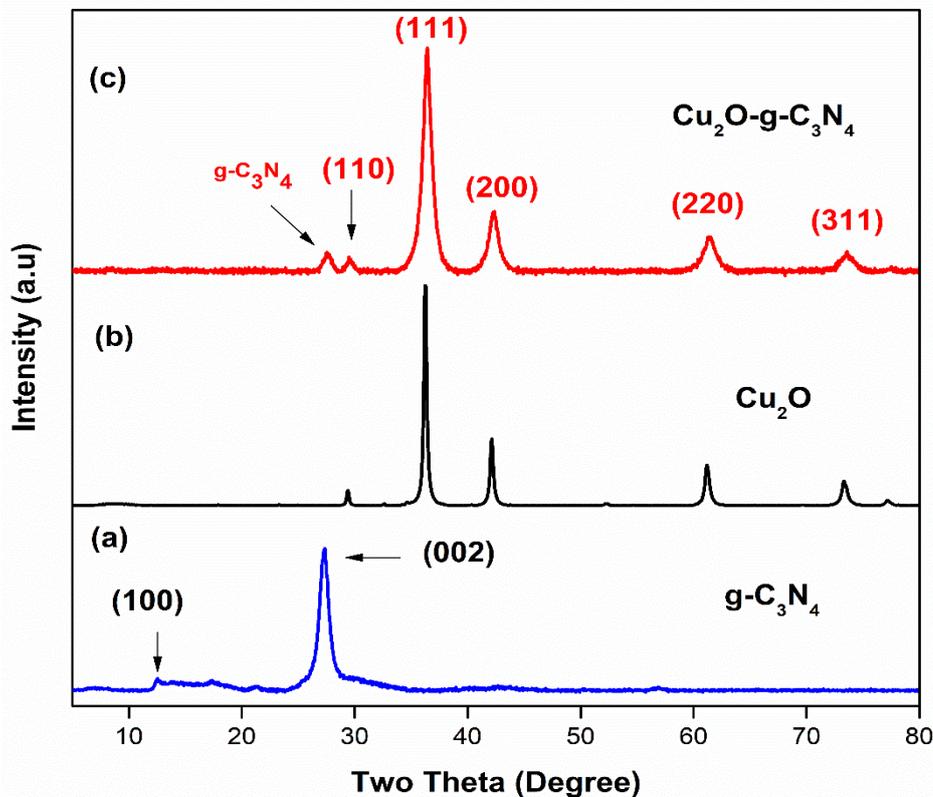
Fig.1: XRD pattern of (a) g-C$_3$N$_4$, (b) Cu$_2$O and (c) Cu$_2$O-g-C$_3$N$_4$ composite material

The FTIR spectra of all the synthesized materials Cu$_2$O, g-C$_3$N$_4$, and Cu$_2$O-g-C$_3$N$_4$ are presented in Fig.2. The peak observed at 620 cm^{-1} in the case of the FTIR spectra of Cu$_2$O (Fig.2(a)) is due to the Cu–O stretching vibrations [58]. Two additional peaks observed at

around 3436 cm^{-1}, and 1643 cm^{-1} are due to the hydroxyl groups of adsorbed water. Similar peaks have also been found in the case of both g-C$_3$N$_4$ and the Cu$_2$O-g-C$_3$N$_4$ composite material. In addition to these peaks, other characteristic peaks observed between 1220-1640 cm^{-1} in the case of g-C$_3$N$_4$ are due to the stretching vibration of connected CN heterocycles (Fig.2(b)) [58]. Another peak that is observed at around 807 cm^{-1} is due to the vibration mode of triazine units as shown in Fig.2(b). The existence of all these characteristic peaks of both g-C$_3$N$_4$ and the Cu$_2$O in the Cu$_2$O- g-C$_3$N$_4$ composite material confirms its synthesis (Fig. 2(c)).
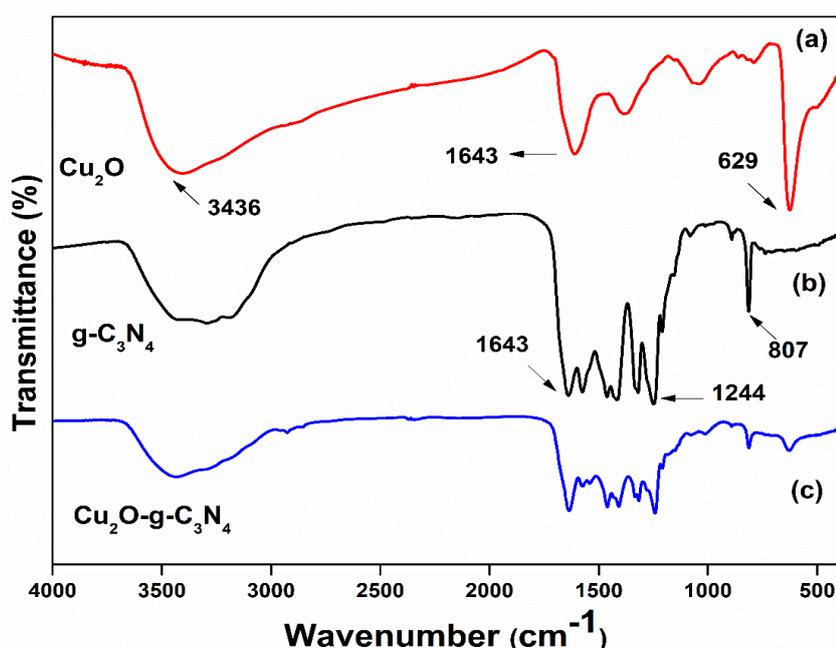
Fig.2: FTIR spectra of (a) Cu$_2$O, (b) g-C$_3$N$_4$ and (c) Cu$_2$O-g-C$_3$N$_4$ composite material

The surface morphology, size of the nanoparticles, elemental composition, and elemental mapping images of all the synthesized materials were obtained from FESEM and EDS analysis. The SEM-EDS analysis and elemental mapping images of both g-C$_3$N$_4$ and Cu$_2$O nanoparticles are provided in supporting information. The FESEM images, as well as EDS along with the mapping of Cu$_2$O- g-C$_3$N$_4$ composite material, are shown in Fig. 3. From the FESEM images (Fig.3(a-b)), it is clearly observed that Cu$_2$O NPs are distributed onto the surface of g-C$_3$N$_4$. The size distribution of Cu$_2$O nanoparticles onto g-C$_3$N$_4$ is found to be in the range of 20-30 nm. The shapes of Cu$_2$O NPs onto g-C$_3$N$_4$ are spherical. The EDS spectrum, as shown in Fig.

3(c) confirms the presence of C, N, O, and Cu in the synthesized Cu_2O- $g-C_3N_4$ composite material without the presence of any impurities. Furthermore, the elemental mapping images of the Cu_2O- $g-C_3N_4$ composite material, as shown in Fig. 3(d-g) presented the homogeneous distribution of Cu, O, C and N in the synthesized composite material.
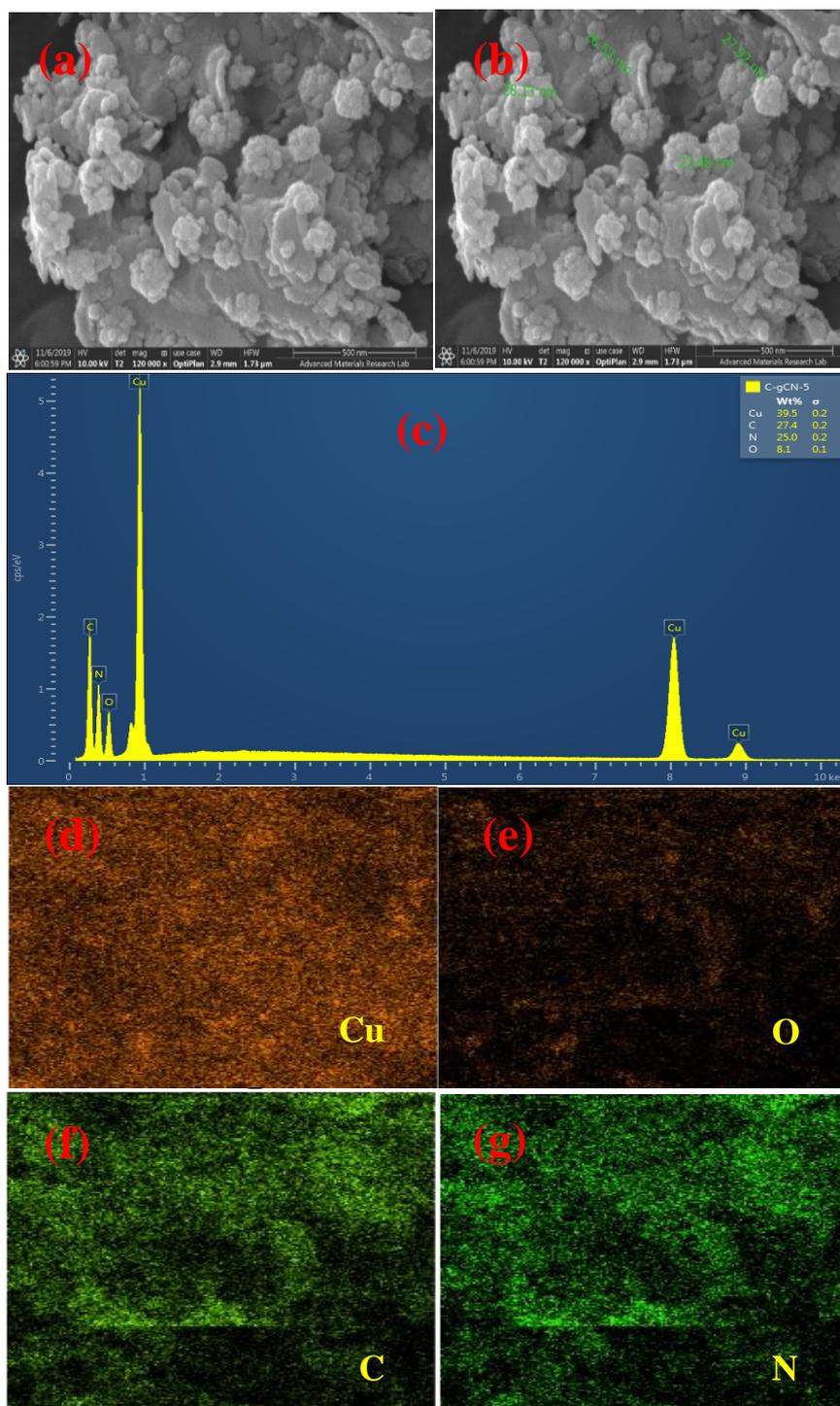
Fig.3: FESEM images (a-b); EDS spectrum (c) and elemental mapping (d-g) of Cu_2O-g-C_3N_4 composite material

XPS analysis was performed to find the chemical state and chemical compositions of the Cu_2O-g-C_3N_4 composite material. The overall XPS spectra of the composite material confirm the presence of Cu, O, N, and C in the Cu_2O- g-C_3N_4 composite material. The C 1s XPS spectrum

of the Cu_2O- g-C_3N_4 composite revealed two major peaks at 284.5 eV and 288.1 eV as shown in Fig. 4(a), which correspond to sp^2 C-C bonds and sp2 bonded carbon in the N-C=N framework, respectively, present in graphitic carbon nitride. The N 1s XPS spectrum survey showed one prominent peak at 398.4 eV, which corresponds to sp^2 bonded N present in the triazine rings of g-C_3N_4 (Fig. 4(b))[58]. Moreover, The Cu 2P XPS spectrum of the Cu_2O- g-C_3N_4 composite material, as shown in Fig. 4(c) displayed two major peaks at the binding energies of 952.8 eV and 933 eV, which corresponds to $2P_{1/2}$ and $2P_{3/2}$, respectively [59]. The appearance of these two major signals arising from the Cu $2P_{3/2}$ and Cu $2P_{1/2}$ confirms the +1 oxidation state of Cu in the synthesized composite material. However, small satellite peaks observed at around 943 eV in the Cu 2P XPS spectrum indicate the presence of a tiny amount of Cu(II) salt, which may be due to the fact that a trace amount of salt is unable to reduce by glucose.
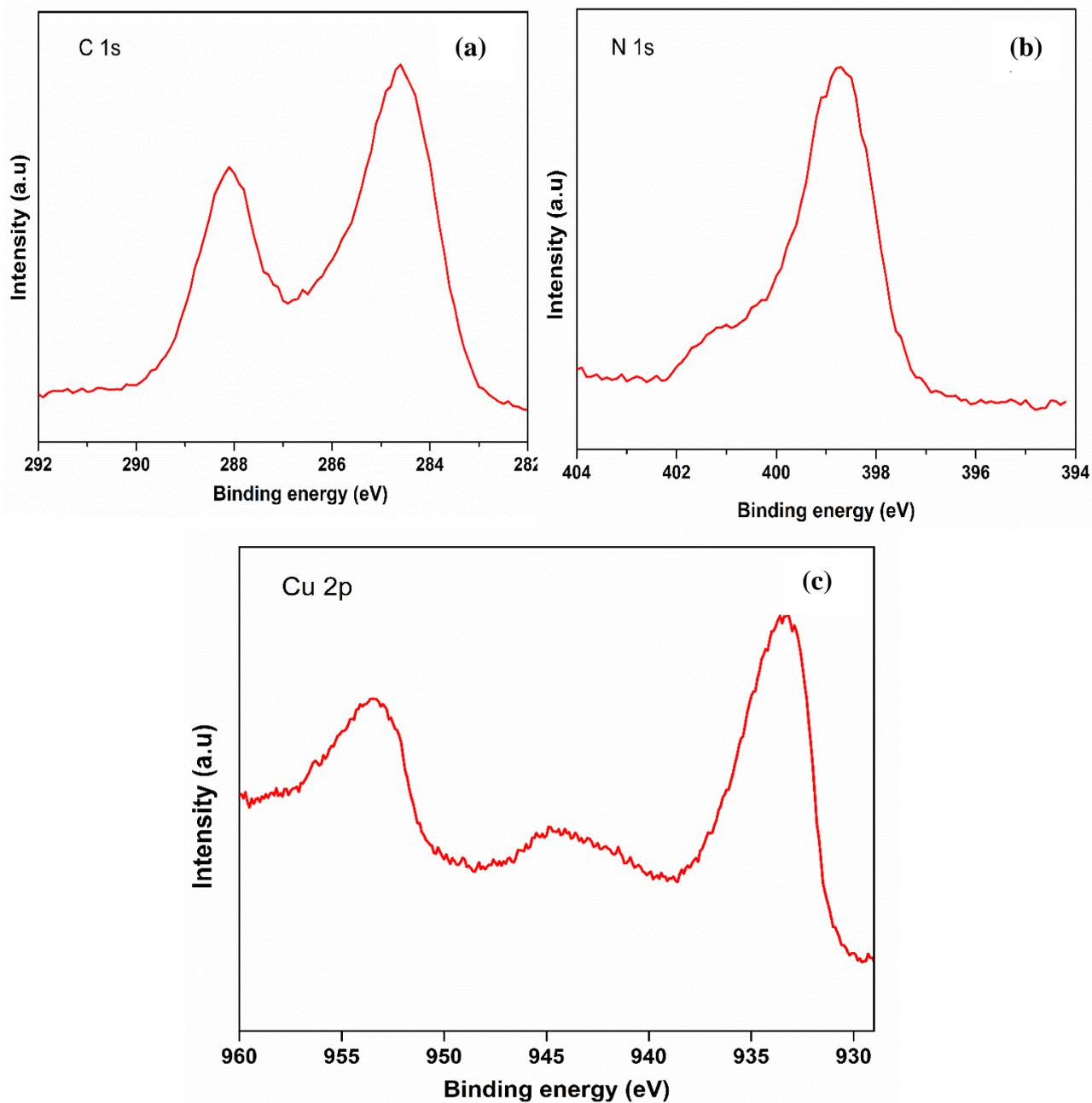
Fig.4: (a) C1s XPS spectrum, (b) N 1s XPS spectrum and (c) Cu 2p XPS spectrum of Cu_2O-g-C_3N_4 composite material

3.2. Electrochemical Performances:

All the prepared materials were first activated in 1 M KOH before determining their electrocatalytic activity at a scan rate of 100 mV/s for 100 cycles. The complete activation of the different samples confirmed from the stable shape of the cyclic voltammograms. Fig. 5 shows the oxidation activity of Cu_2O NPs compared to that supported on g-C_3N_4 and that of g-

C$_3$N$_4$. As being clear from the figure that Cu$_2$O NPs supported on g-C$_3$N$_4$ demonstrated superior oxidation activity towards urea compared to that of unsupported Cu$_2$O, while g-C$_3$N$_4$ showed no activity towards urea oxidation as clear from the almost zero current generation during the measurements. For instance, at 0.5 V vs. Ag/AgCl, the current density in the case of Cu$_2$O-g-C$_3$N$_4$ is 5.5 mAcm^{-2}, which is two times that of obtained in case of the unsupported Cu$_2$O at the same voltage.
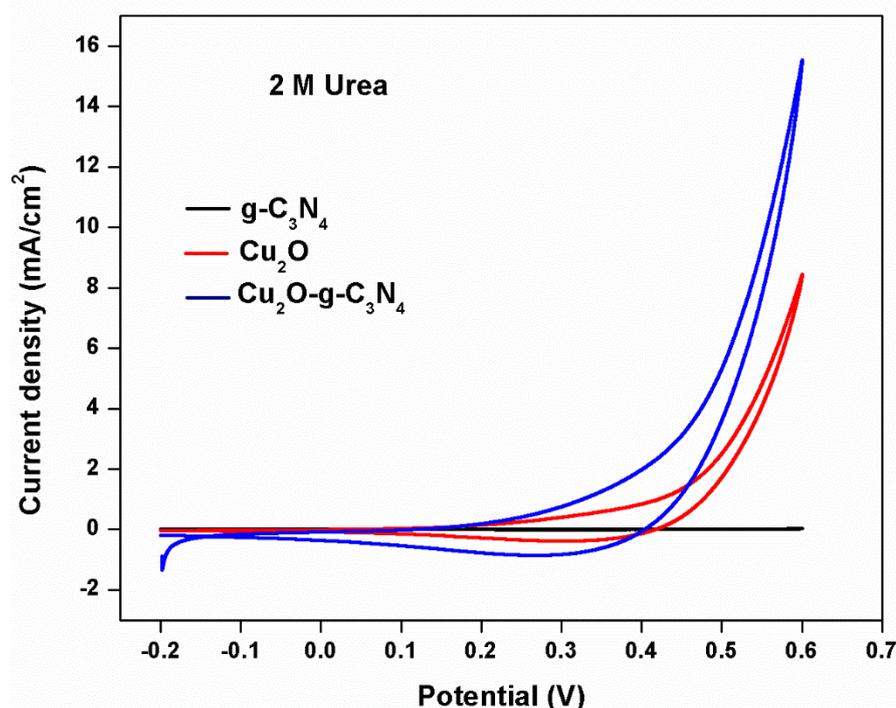
Fig.5: CV of g-C$_3$N$_4$, Cu$_2$O, and Cu$_2$O- g-C$_3$N$_4$ composite (4.8 mgcm^{-2}) using 2 M Urea concentration

Fig. 6(a-e) shows the oxidation activity of Cu$_2$O-g-C$_3$N$_4$ of different loading of 1.4, 2.8, 4.2, and 5.6 mgcm^{-2} using different concentrations of urea of 0.1 M (Fig. 6a), 0.33 M (Fig. 6b), 0.5 M (Fig. 6c), 1 M (Fig. 6d), and 2M (Fig. 6e) in 1M KOH. It is clear from the figure that regardless of the urea concentration, the oxidation activity, i.e., the current generated in the forward scan, increases with increasing the catalyst loading from 1.4 mgcm^{-2} to 4.2 mgcm^{-2}, While the activity decreases with the further increase in the catalyst loading to 5.6 mgcm^{-2}. This behavior could be related to the following: At low catalyst loading, the number of the

active sites is few, and the distance between the active sites is relatively high compared with the higher catalyst loadings, and thus the increase of the loading from 1.4 to 4.2 mgcm^{-2} results in improving the performance. While the further increase in the catalyst loading to 5.6 mgcm^{-2} results in the formation of a thick catalyst layer that would obstruct both the mass transfer and the charge transfer, and thus performance decreases. Fig. 6f shows the oxidation activity of the Cu$_2$O-g-C$_3$N$_4$ of 4.2 mgcm^{-2} using different concentrations of urea from 0 M to 2 M. As being clear from the figure that the current increases with increasing the urea from 0 M to 1 M then it is nearly constat at 2 M. Also, it is clear that the onset potential (potential at which the urea oxidation current is generated compared to the case of urea free KOH) is 0.37 V which is similar to that reported for Ni and Ni catalyst alloys [60, 61].
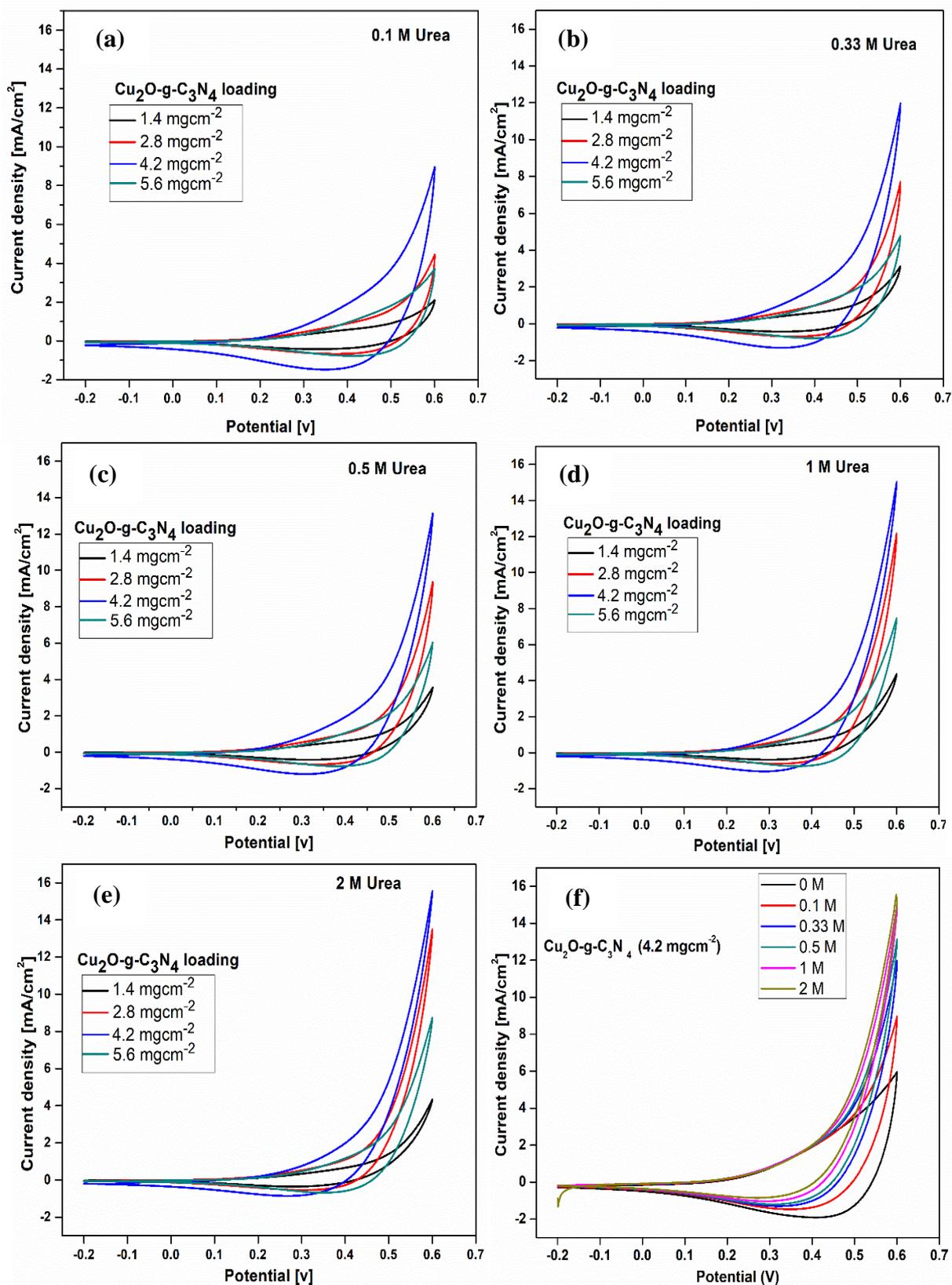
Fig.6: (a-e) CV of different amount of Cu₂O- g-C₃N₄ composite such as 1.4, 2.8, 4.2 and 5.6 mgcm⁻² using various concentrations of urea like 0, 0.1, 0.33, 0.5, 1 and 2 M, and (f) the effect of concentration of urea on the activity of Cu₂O-g-C₃N₄ at 4.8 mgcm⁻².

Electrochemical impedance spectroscopy (EIS) is an effective method to show the effect of the catalyst loading on ohmic resistance, mass transfer resistance, and charge transfer resistance. The effect of the catalyst loading on the EIS using 2 M urea is presented in Fig.7. As seen from the inset in the figure (intersection with the X-axis) that the ohmic resistance increased when catalyst loading is increased that is following the ohmic law. While the increase of the catalyst loading resulted in improving both the charge transfer and mass transfer, as seen from the decrease of the radius of the medium and low frequencies, respectively. However, the increase of the catalyst loading beyond the 4.8 mgcm^{-2}, the mass transfer resistivity is increased. This behavior could be correlated to the increase of the active sites over the glassy carbon electrode surface as well as the decrease of the distance between the individual particles. However, at a high catalyst loading of the catalyst, i.e., 5.6 mgcm^{-2}, a too thick layer of the catalyst formed over the surface, and thus the mass transfer resistivity is appeared. Both of the increase in the ohmic resistance with increasing the catalyst loading as well as the imperfect mass transfer at 5.6 mgcm^{-2} catalyst loading resulted in decreasing the performance.
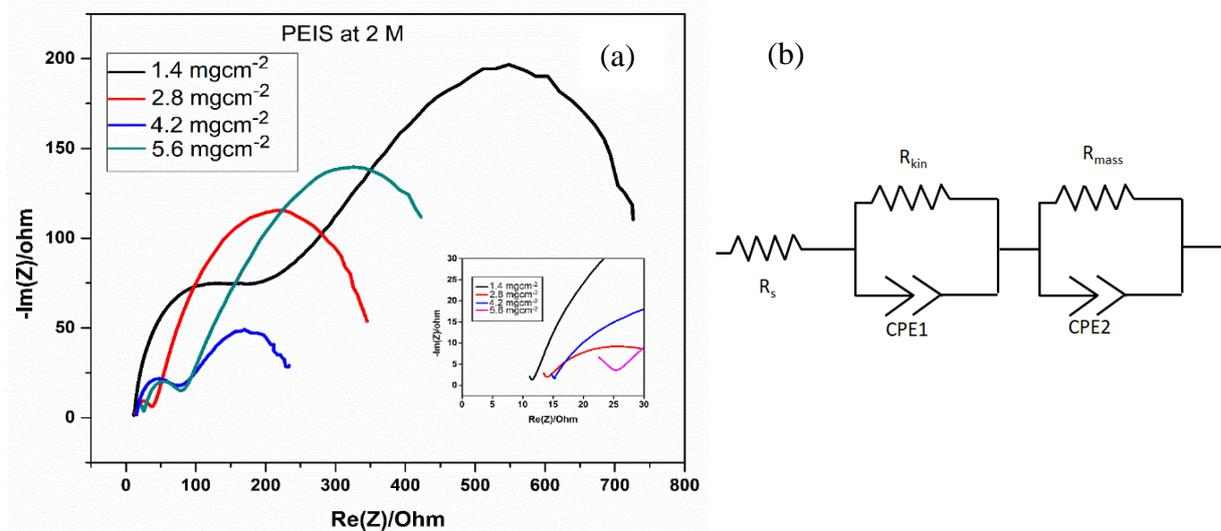
Fig.7: (a) Electrochemical impedance spectroscopy (EIS) of different amount of CuO-g-C$_3$N$_4$ composite using 2M urea; (b) The equivalent circuit of the bode plot composed of ohmic resistance and charge transfer resistance

The equivalent circuit of the bode circuit is composed of ohmic resistance (R_s) that clear from the intersection at high frequency with the X-axis (inset of Fig. 7), the semi circuit appears at medium frequency is modeled by double layer capacitance (CPE1) in parallel to charge transfer resistance (R_{kin}), and the semicircuit at the low frequency is modeled by a another double layer capacitance (CPE2) that is in parallel to mass transfer resistance (R_{mass}) [62] as can be seen in Fig. 7b.

Performing cyclic voltammetry at different scan rate is an effective way for determining whether the rate of the reaction is diffusion-controlled (linear dependence of the anodic peak current density and on the square root of the scan rate) or kinetic controlled (linear dependence of the anodic peak potential on the logarithm of the scan rate). As can be seen in Fig 8(a) and 8(b) that the reaction is diffusion-controlled and not kinetics controlled as clear from the linear dependence of the current density at 0.5 V vs Ag/AgCl on the square root of the scan rate (Fig. 8a), while there is no dependence of the anodic potential (at 10 mAcm^{-2}) on the logarithm of the scan rate (Fig.8b). Where the linear sweep voltammetry is just showing the instantaneous performance and not showing the variation of the performance with time, the current discharge at a constant voltage of 0.5 V vs Ag/AgCl for 200 minutes. As seen in Fig. 9, the performance is stable with no noticeable degradation in the performance, indicating that the high stability of the catalyst, and its ability to be used under real fuel cell application. The Cu_2O prepared on the surface of g-C_3N_4 exhibited the best performance, which is more than twice that of the unsupported Cu_2O, while g-C_3N_4 had no activity in the oxidation of urea. The resulted higher activity of the composite material is due to the synergistic effect of their individual components.
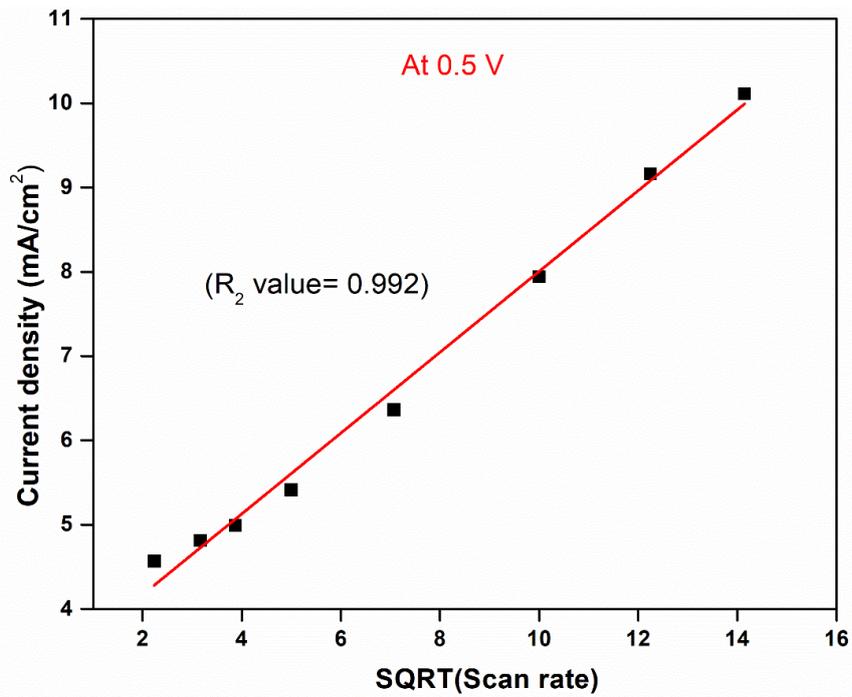
Fig.8(a): Effect of SQRT of scan rate on the efficiency of CuO-g-C₃N₄ composite (4.8 mgcm⁻²) in 2 M concentration of urea
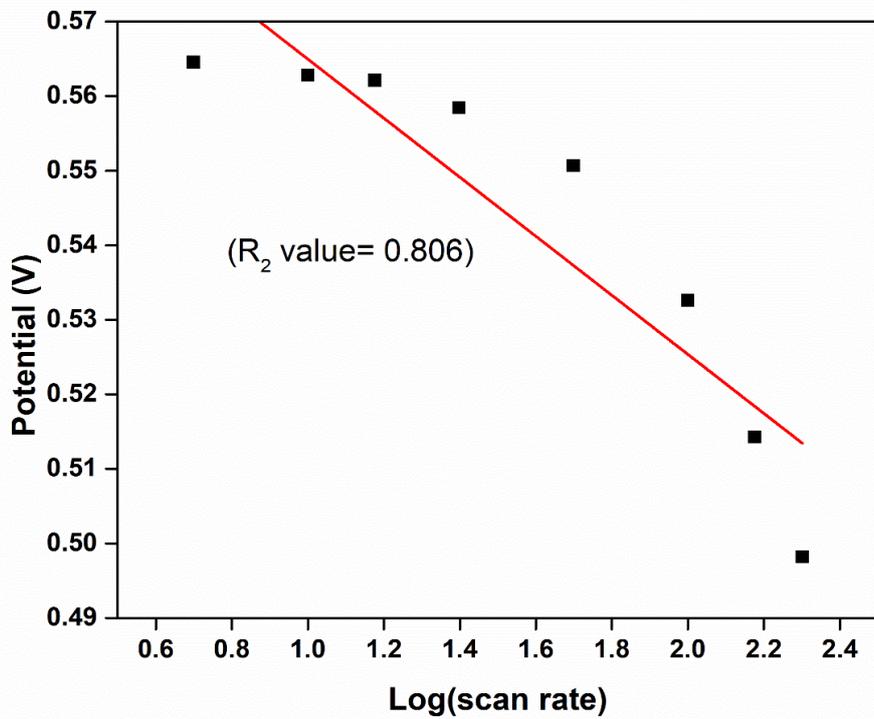
Fig.8(b): Log of scan rate vs potential at 10 mAcm^{-2} of CuO-g-C₃N₄ composite (4.8 mgcm^{-2}) in 2 M concentration of Urea
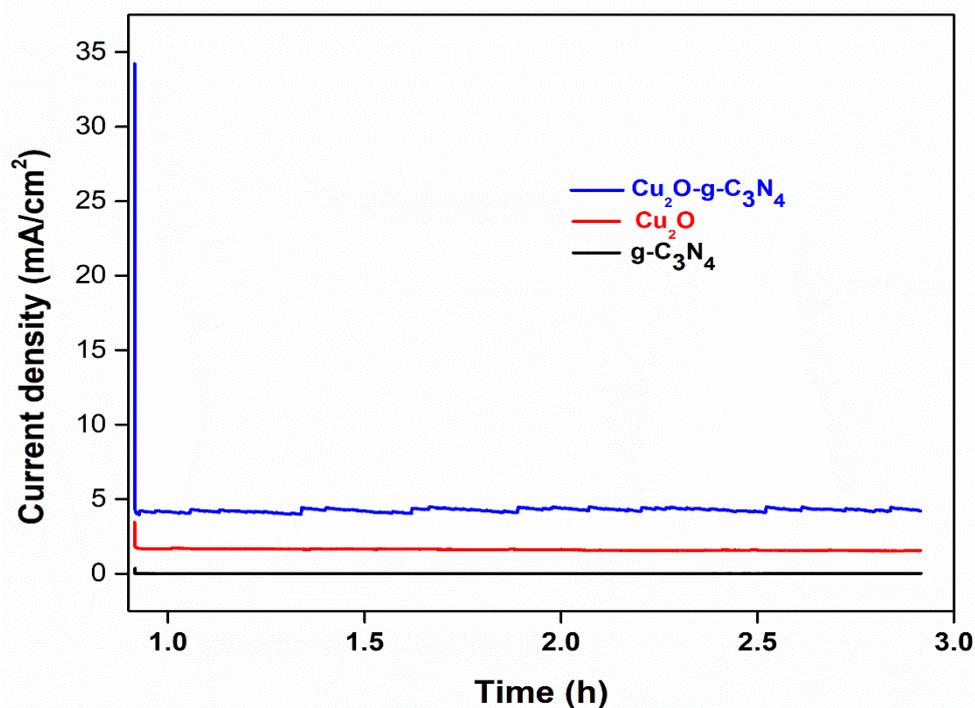
Fig.9: Chronoamperometric measurement of g-C$_3$N$_4$, Cu$_2$O, and Cu$_2$O- g-C$_3$N$_4$ composite material using 2M urea in 1 M KOH

Again, the Chronoamperometric measurement of the Cu$_2$O-g-C$_3$N$_4$ with various catalytic loading of 1.4 mgcm^{-2}, 2.8 mgcm^{-2} and 4.2 mgcm^{-2} using 2 M urea were done to further prove the stability of the synthesized two dimensional Cu$_2$O-g-C$_3$N$_4$ composite material. It is found that the composite material irrespective of their catalytic loading exhibited high stability as shown in (Fig. 10(a)). In addition to these, the Chronoamperometric measurement of Cu$_2$O-g-C$_3$N$_4$ with 4.2 mgcm^{-2} catalytic loading at 2 M urea proved that the composite is highly stable up to 10 h without any noticeable degradation in the performance as shown in (Fig. 10(b)).
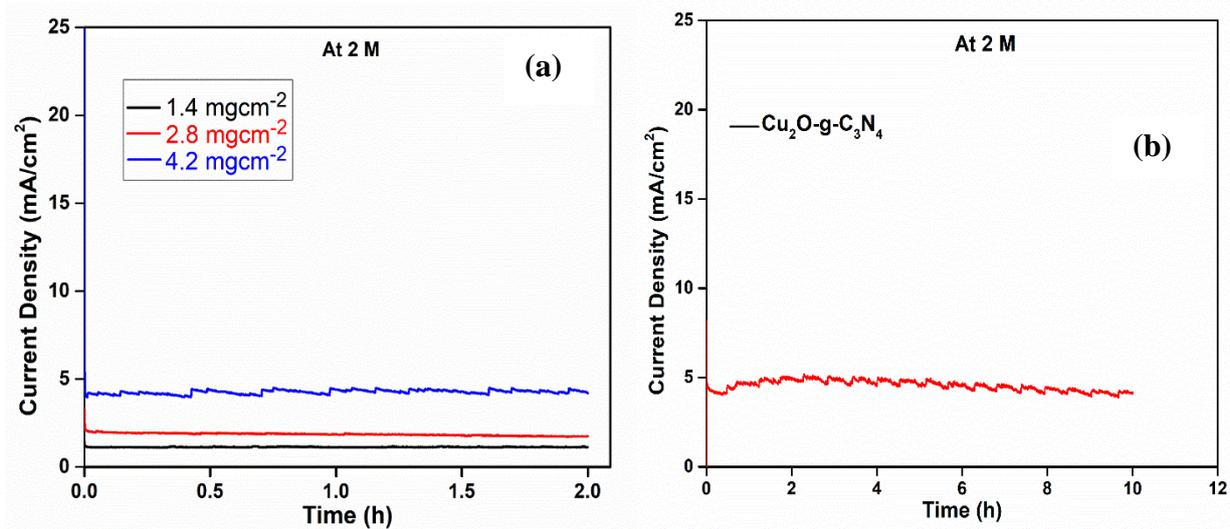
Fig.10: Chronoamperometric measurement of (a) Cu_2O- g-C_3N_4 composite with different catalytic loading and (b) Cu_2O- g-C_3N_4 composite with catalytic laoding of 4.2 mgcm^{-2} for 10 h using 2 M urea

4. Conclusions:

In conclusion, g-C_3N_4, Cu_2O, and Cu_2O-g-C_3N_4 were successfully synthesized by adopting a simple solution chemistry approach using an environmentally friendly reducing agent. The synthesized materials were characterized by different instrument techniques such as XPS, XRD, FESEM, EDX, and FTIR. Further, the synthesized materials were investigated as electrocatalyst in the urea oxidation. The composite material was found to be much more efficient electrocatalyst in comparison to g-C_3N_4 and Cu_2O alone due to their synergistic effect between the Cu_2O and the g-C_3N_4. The activity of different catalyst loading from 1.4 to 5.6 mgcm^{-2} of the catalyst Cu_2O- g-C_3N_4, towards urea oxidation was also investigated. The catalyst loading of 4.8 exhibited the best performance due to the increase in the number of active sites without a significant increase in the ohmic resistance. This report is the first one for using g-C_3N_4 as support for Cu_2O NPs in fuel cell applications.

References:

[1] J. Ren, Y.-L. Liu, X.-Y. Zhao, J.-P. Cao, International Journal of Hydrogen Energy, 45 (2020) 4223-4243.

[2] T. Bak, J. Nowotny, M. Rekas, C.C. Sorrell, International Journal of Hydrogen Energy, 27 (2002) 991-1022.

[3] F. Yilmaz, M. Ozturk, R. Selbas, International Journal of Hydrogen Energy, 43 (2018) 10626-10636.

[4] H. Ishaq, I. Dincer, International Journal of Hydrogen Energy, (2020).

[5] B. Pandey, Y.K. Prajapati, P.N. Sheth, International Journal of Hydrogen Energy, 44 (2019) 25384-25415.

[6] Y. Zheng, L. Tao, X. Yang, Y. Huang, C. Liu, Z. Zheng, International Journal of Hydrogen Energy, 43 (2018) 16479-16496.

[7] R.A. Voloshin, M.V. Rodionova, S.K. Zharmukhamedov, T. Nejat Veziroglu, S.I. Allakhverdiev, International Journal of Hydrogen Energy, 41 (2016) 17257-17273.

[8] K. Urbaniec, M. Markowski, A. Budek, International journal of hydrogen energy, 39 (2014) 7468-7475.

[9] M.H. Karimi, N. Chitgar, M.A. Emadi, P. Ahmadi, M.A. Rosen, International Journal of Hydrogen Energy, 45 (2020) 6262-6277.

[10] R.M. Abdel Hameed, S.S. Medany, International Journal of Hydrogen Energy, 44 (2019) 3636-3648.

[11] M.S. Seong, C.I. Kong, B.R. Park, Y. Lee, B.K. Na, J.H. Kim, Chemical Engineering Journal, 384 (2020) 123342.

[12] M.A. Abdelkareem, W.H. Tanveer, E.T. Sayed, M.E.H. Assad, A. Allagui, S. Cha, Renewable and Sustainable Energy Reviews, 101 (2019) 361-375.

[13] M.A. Abdelkareem, A. Allagui, T. Tsujiguchi, N. Nakagawa, Journal of The Electrochemical Society, 163 (2016) F1011-F1016.

[14] N. Nakagawa, M.A. Abdelkareem, T. Tsujiguchi, M.S. Mastar, DMFC with a fuel transport layer using a porous carbon plate for neat methanol use, Direct Methanol Fuel Cells: Applications, Performance and Technology, Nova Science Publishers, Inc.2017, pp. 51-95.

[15] M.A. Abdelkareem, M.S. Masdar, T. Tsujiguchi, N. Nakagawa, E.T. Sayed, N.A. Barakat, Chemical Engineering Journal, 240 (2014) 38-44.

[16] K. Ng, H. Rahman, M.R. Somalu, International Journal of Hydrogen Energy, 44 (2019) 30692-30704.

[17] A. Veziroglu, R. Macario, International Journal of Hydrogen Energy, 36 (2011) 25-43.

[18] X. Ren, Q. Lv, L. Liu, B. Liu, Y. Wang, A. Liu, G. Wu, Sustainable Energy & Fuels, 4 (2020) 15-30.

[19] S. Yu, F. Li, H. Yang, G. Li, G. Zhu, J. Li, L. Zhang, Y. Li, International Journal of Hydrogen Energy, 42 (2017) 29971-29976.

[20] M.A. Abdelkareem, E.T. Sayed, H.O. Mohamed, M. Obaid, H. Rezk, K.-J. Chae, Progress in Energy and Combustion Science, 77 (2020) 100805.

[21] E.T. Sayed, T. Eisa, H.O. Mohamed, M.A. Abdelkareem, A. Allagui, H. Alawadhi, K.-J. Chae, Journal of Power Sources, 417 (2019) 159-175.

[22] R.A. Hameed, S.S. Medany, International Journal of Hydrogen Energy, 44 (2019) 3636-3648.

[23] R.A. Hameed, S.S. Medany, International Journal of Hydrogen Energy, 42 (2017) 24117-24130.

[24] K. Ye, D. Zhang, F. Guo, K. Cheng, G. Wang, D. Cao, Journal of Power Sources, 283 (2015) 408-415.

[25] R.-Y. Ji, D.-S. Chan, J.-J. Jow, M.-S. Wu, Electrochemistry communications, 29 (2013) 21-24.

[26] F. Guo, K. Ye, K. Cheng, G. Wang, D. Cao, Journal of Power Sources, 278 (2015) 562-568.

[27] L. Bian, Q. Du, M. Luo, L. Qu, M. Li, International Journal of Hydrogen Energy, 42 (2017) 25244-25250.

[28] D. Wang, W. Yan, S.H. Vijapur, G.G. Botte, Electrochimica Acta, 89 (2013) 732-736.

[29] N.A. Barakat, M. Motlak, Z.K. Ghouri, A.S. Yasin, M.H. El-Newehy, S.S. Al-Deyab, Journal of Molecular Catalysis A: Chemical, 421 (2016) 83-91.

[30] W. Yan, D. Wang, G.G. Botte, Applied Catalysis B: Environmental, 127 (2012) 221-226.

[31] W. Yan, D. Wang, G.G. Botte, Electrochimica Acta, 61 (2012) 25-30.

[32] M.A. Abdelkareem, Y. Al Haj, M. Alajami, H. Alawadhi, N.A. Barakat, Journal of environmental chemical engineering, 6 (2018) 332-337.

[33] M. Alajami, M.A. Yassin, Z.K. Ghouri, S. Al-Meer, N.A. Barakat, International Journal of Hydrogen Energy, 43 (2018) 5561-5575.

[34] W. Xu, D. Du, R. Lan, J. Humphreys, Z. Wu, S. Tao, New Journal of Chemistry, 41 (2017) 4190-4196.

[35] R.H. Tammam, H. Hassan, Journal of The Electrochemical Society, 166 (2019) F729-F745.

[36] T.Q.N. Tran, B.J. Park, W.H. Yun, T.N. Duong, H.H. Yoon, Scientific Reports, 10 (2020) 1-10.

[37] M.H. Tran, B.J. Park, B.H. Kim, H.H. Yoon, International Journal of Hydrogen Energy, 45 (2020) 1784-1792.

[38] E. Urbańczyk, A. Maciej, W. Simka, International Journal of Hydrogen Energy, 45 (2020) 1769-1783.

[39] A. Galal, N.F. Atta, M.A. Hefnawy, Journal of Electroanalytical Chemistry, (2020) 114009.

[40] G. Ma, Q. Xue, J. Zhu, X. Zhang, X. Wang, H. Yao, G. Zhou, Y. Chen, Applied Catalysis B: Environmental, 265 (2020) 118567.

[41] W. Shi, J. Lian, Materials Chemistry and Physics, 242 (2020) 122517.

[42] S.-B. Yang, Y.-C. Tsai, M.-S. Wu, Journal of Alloys and Compounds, (2020) 155533.

[43] S.N. Azizi, S. Ghasemi, E. Chiani, Electrochimica Acta, 88 (2013) 463-472.

[44] M. Hosseini, M. Momeni, M. Faraji, Electroanalysis, 22 (2010) 2620-2625.

[45] Y. Luo, Y. Yan, S. Zheng, H. Xue, H. Pang, Journal of materials chemistry A, 7 (2019) 901-924.

[46] P. Zhang, F. Wang, M. Yu, X. Zhuang, X. Feng, Chemical Society Reviews, 47 (2018) 7426-7451.

[47] K.S. Novoselov, A.K. Geim, S.V. Morozov, D. Jiang, Y. Zhang, S.V. Dubonos, I.V. Grigorieva, A.A. Firsov, science, 306 (2004) 666-669.

[48] M. Xu, T. Liang, M. Shi, H. Chen, Chemical reviews, 113 (2013) 3766-3798.

[49] J. Low, S. Cao, J. Yu, S. Wageh, Chemical communications, 50 (2014) 10768-10777.

[50] Z. Zhao, Y. Sun, F. Dong, Nanoscale, 7 (2015) 15-37.

[51] X. Wang, S. Blechert, M. Antonietti, Acs Catalysis, 2 (2012) 1596-1606.

[52] N. Mansor, T.S. Miller, I. Dedigama, A.B. Jorge, J. Jia, V. Brázdová, C. Mattevi, C. Gibbs, D. Hodgson, P.R. Shearing, Electrochimica Acta, 222 (2016) 44-57.

[53] G. Darabdhara, M.R. Das, Chemosphere, 197 (2018) 817-829.

[54] Y. Zheng, J. Liu, J. Liang, M. Jaroniec, S.Z. Qiao, Energy & Environmental Science, 5 (2012) 6717-6731.

[55] J. Zhu, P. Xiao, H. Li, S.A. Carabineiro, ACS applied materials & interfaces, 6 (2014) 16449-16465.

[56] C. Ji, S.-N. Yin, S. Sun, S. Yang, Applied Surface Science, 434 (2018) 1224-1231.

[57] S. Zuo, H. Xu, W. Liao, X. Yuan, L. Sun, Q. Li, J. Zan, D. Li, D. Xia, Colloids and Surfaces A: Physicochemical and Engineering Aspects, 546 (2018) 307-315.

[58] S. Anandan, J.J. Wu, D. Bahnemann, A. Emeline, M. Ashokkumar, Colloids and Surfaces A: Physicochemical and Engineering Aspects, 527 (2017) 34-41.

[59] D. Zhao, C.-M. Tu, X.-J. Hu, N. Zhang, RSC advances, 7 (2017) 37596-37603.

[60] T. Eisa, H.O. Mohamed, Y.-J. Choi, S.-G. Park, R. Ali, M.A. Abdelkareem, S.-E. Oh, K.-J. Chae, International Journal of Hydrogen Energy, 45 (2020) 5948-5959.

[61] N.A.M. Barakat, M. Ali Abdelkareem, E.A.M. Abdelghani, Catalysts, 9 (2019) 330.

[62] D.E. Glass, V. Galvan, G.K.S. Prakash, Electrochimica Acta, 253 (2017) 489-497.